



**HAL**  
open science

## Lignocellulosic fiber breakage in a molten polymer. Part 2. Quantitative analysis of the breakage mechanisms during compounding

Erika Di Giuseppe, Romain Castellani, Tatiana Budtova, Bruno Vergnes

### ► To cite this version:

Erika Di Giuseppe, Romain Castellani, Tatiana Budtova, Bruno Vergnes. Lignocellulosic fiber breakage in a molten polymer. Part 2. Quantitative analysis of the breakage mechanisms during compounding. *Composites Part A: Applied Science and Manufacturing*, 2017, 95, pp.31-39. 10.1016/j.compositesa.2016.12.011 . hal-04057679

**HAL Id: hal-04057679**

**<https://hal.science/hal-04057679>**

Submitted on 4 Apr 2023

**HAL** is a multi-disciplinary open access archive for the deposit and dissemination of scientific research documents, whether they are published or not. The documents may come from teaching and research institutions in France or abroad, or from public or private research centers.

L'archive ouverte pluridisciplinaire **HAL**, est destinée au dépôt et à la diffusion de documents scientifiques de niveau recherche, publiés ou non, émanant des établissements d'enseignement et de recherche français ou étrangers, des laboratoires publics ou privés.

**Lignocellulosic fiber breakage in a molten polymer. Part 2. Quantitative  
analysis of the breakage mechanisms during compounding**

E. Di Giuseppe, R. Castellani, T. Budtova, B. Vergnes\*

MINES ParisTech, PSL Research University, CEMEF (Centre de Mise en Forme des  
Matériaux), UMR CNRS 7635, CS 10207, 06904 Sophia Antipolis Cedex, France

Corresponding author :

Bruno Vergnes, email : [Bruno.Vergnes@mines-paristech.fr](mailto:Bruno.Vergnes@mines-paristech.fr)

Tel.: (+33) 4 93 95 74 63

## **Abstract**

Composites made of polypropylene and short lignocellulosic fibers are usually produced by compounding in a twin-screw extruder. During processing, fibers are submitted to stress and strain and they undergo severe degradations, i.e. a reduction of both length and diameter, affecting the final properties of the composites. In this paper, which is the second of a series, we have systematically studied the changes in the dimensions of four different types of fibers (hemp, miscanthus, sisal, flax) under different processing conditions, using an internal mixer to mimic the extrusion process. We show that the fibers' length and diameter decrease with the strain cumulated during the process. These changes may be described using exponential laws, the parameters of which differ from one fiber type to another. Based on these evolution laws, we propose to define a "breakage index" to discriminate the behavior of the different types of fibers.

**Keywords:** A. Polymer-matrix composites; A. Short-fibers composites; B. Fragmentation; E. Compounding

## **1. Introduction**

From an industrial point of view, the preparation of thermoplastic composites reinforced with short lignocellulosic fibers is done primarily by compounding in twin-screw extruders, although we may also find in the literature a few examples using single-screw extruders [1] or Buss co-kneaders [2]. The intrinsic properties of lignocellulosic fibers make them an interesting reinforcement potential that must be preserved during the preparation of the composite [3]. Particularly, it is important to maintain as high as possible the length ( $L$ ) and the aspect ratio (length/diameter,  $L/D$ ) of the fibers in order to obtain competitive mechanical properties in the final material [4, 5].

It is well known that lignocellulosic fibers submitted to a thermomechanical treatment undergo a decrease in both diameter (dissociation of bundles into individual fibers) and length (breakage of bundles and single fibers) [6-12]. The mechanisms of dissociation and breakage depend on the plant species and have been qualitatively observed in the first paper of this series [13]. For example, it was shown that hemp breaks after numerous bending, flax shows mixed fatigue and fragile behavior, and miscanthus and sisal bundles are “peeled”. It is also known that in the case of flax the breakage is preferentially located at points of weakness (called “kink bands” or “knees”), along the elementary fibers [14-16]. In order to control the quality of the final composite parts, it is therefore essential to understand how these mechanisms of breakage occur quantitatively, what the parameters that govern them are, and how to limit them to preserve the fiber reinforcement properties. This is the goal of the present paper.

Of course, many parameters play a role in the breakage mechanisms, like fiber composition (respective amount of cellulose, hemicellulose, pectin, lignin, etc.), but also fiber morphology (lumen size, cell wall thickness, microfibril angle, etc.). Even

though all these parameters are important, it is not possible to check the effect of each of them. In the following, we will only select four different types of fibers, and present a methodology leading to quantitative evolution laws, able to describe in a general way the breakage of these fibers.

For this, we conducted a study of the size evolution of four different types of fibers in composites prepared using an internal mixer. These fibers (hemp, miscanthus, sisal, and flax) have shown different breakage mechanisms in rheo-optical observations [13] and thus, one should expect various size evolution kinetics during compounding. In the literature, the internal mixer is often used to prepare composites with lignocellulosic fibers [7, 8, 17-19]. Quijano-Solis et al. [20] studied the influence of the rotation speed, of the fiber content, and of the barrel temperature on the size of aspen fibers and corn straw, like did Joseph et al. [21] on sisal fibers. Baiardo et al. [22] characterized the effects of rotor speed and mixing time on flax fibers, as Iannace et al. [23] on sisal fibers. However, these studies are usually limited to a reduced range of processing parameters and a small number of fiber types. Moreover, clear relationships between process parameters and fiber size changes are almost never reported.

## **2. Materials and Methods**

### *2.1 Fibers and fiber size analysis*

Four types of fibers were considered: retted hemp, sisal, miscanthus, and flax. The first three fibers are rather short (from 1.9 to 3.5 mm); the latter is longer (12 mm). These dimensions are usually encountered when preparing composites for subsequent injection molding. The bundles are made of elementary fibers maintained together by an "interfiber cement", consisting essentially of amorphous polymers (lignin, hemicellulose, pectin) and the bio-chemical composition of which is unique for each

species [13]. The contents of lignin and hemicellulose in the fibers studied are provided in Table 1.

The initial dimensions of the fibers are also shown in Table 1. SEM pictures of the four types of fibers are presented in Supplementary Data (Fig. S1). The size distributions, in length  $L$ , diameter  $D$  and aspect ratio  $L/D$ , were quantified using a high resolution scanner (Epson Perfection<sup>TM</sup> V550 Photo Color), in transmission mode and with a resolution of 6400 dpi, corresponding to 4  $\mu\text{m}/\text{pixel}$ ; the image analysis software was ImageJ [24]. From these distributions, we can calculate average values. In the following, we focus on the weight average values, which give more significance to the higher values of the distributions. They are defined by:

$$L_w = \frac{\sum_{i=1}^{N_c} n_i L_i^2}{\sum_{i=1}^{N_c} n_i L_i}, \quad D_w = \frac{\sum_{i=1}^{N_c} n_i D_i^2}{\sum_{i=1}^{N_c} n_i D_i}, \quad (L/D)_w = \frac{\sum_{i=1}^{N_c} n_i (L/D)_i^2}{\sum_{i=1}^{N_c} n_i (L/D)_i} \quad (1)$$

where  $N_c$  is the number of classes of the distribution, and  $n_i$  is the number of fibers of length  $L_i$  (diameter  $D_i$  and aspect ratio  $(L/D)_i$ , respectively). The sizes after compounding were quantified using the same methodology (scanner and image analysis) after dissolving the matrix in Decalin<sup>®</sup> (decahydronaphthalene). More details in the measurement and analysis of fiber sizes are provided by Di Giuseppe et al. [24].

## 2.2 Matrix

Two homopolymer polypropylenes (PP) were used to vary matrix viscosity: PPH5060, purchased from Total Petrochemicals, with a melt flow index (MFI) of 6 g/10 min (230 °C, 2.16 kg), and Moplen HP400R, provided by LyondellBasel, with MFI of 25 g/10 min. PPH5060 is thus more viscous than HP400R. The complex viscosity curves at 180 °C of both PP are presented in Supplementary Data, Figure S2.

A good interfacial adhesion between fibers and matrix is essential in order to obtain interesting mechanical properties. To improve it, we used a maleic anhydride grafted polypropylene (PP-g-MA) as compatibilizer. It has a melt index higher than 50 g/10 min (230 °C, 2.16 kg), and a density of 910 kg/m<sup>3</sup>. We selected the recommended value of 1/10 by weight for the PP-g-MA/fibers ratio [7, 19, 25]. The composition of the composites was kept constant during this study and was set as follows: 78 wt% PP/ 2 wt% PP-g-MA/ 20 wt% fibers.

### 2.3 Internal mixer

All composites have been prepared using an internal mixer Haake Rheomix 600, equipped with "roller" rotors, following the same protocol. The control temperature of the mixing chamber was fixed at 180 °C. The changes in product temperature and torque were recorded during the experiments. An example of the experimental curves is shown in Figure 1a. At time  $t = 0$ , the pre-blended pellets of PP and PP-g-MA were introduced in the chamber and melted for two minutes at 100 rpm (phase 1). Then the speed was reduced to 50 rpm for 5 minutes during which fibers were added (phase 2). This was done in five steps, because of the large volume represented by the 20 wt% fibers. At the end of phase 2, the mixing phase itself started (phase 3), for which we varied systematically the rotation speed (from 25 to 200 rpm) and the mixing time (from 1 to 5 minutes). This range of values corresponds to what could be usually encountered in an extrusion process. During this last phase, the torque decreased and tended to stabilize while the temperature increased due to viscous dissipation. In the case presented in Figure 1a (hemp fibers, 5 min, 200 rpm), the final temperature reached 210 °C (i.e. 30 °C higher than the control temperature). Figure 2 shows the temperatures reached at the end of mixing as a function of the operating conditions, i.e. rotor speed and mixing time, for the sisal based composites. An increase in temperature is observed

with both time and speed, with a stabilization at long times. High speeds lead to significant overheating, up to 40 °C above the control temperature, which could be detrimental to the quality of the fibers, which are known to degrade at high temperatures [20, 26].

Figure 1b shows, for the same case as shown in Figure 1a, the time evolution of the mechanical energy applied to the material, calculated from the torque. The mechanical energy does not vary much during the fibers' introduction (phase 2) and most of it is transmitted to the composite during the mixing stage (phase 3).

To characterize the thermomechanical treatment applied to the fibers, several parameters, commonly used in the literature [5, 15, 27], can be defined. The first one is the specific mechanical energy (*SME*), which is expressed as:

$$SME = \frac{1}{m} \int_0^t C(t)Ndt \quad (2)$$

where  $C$  is the torque,  $N$  is the rotor speed, and  $m$  is the mass introduced in the mixer.

The second parameter is the cumulative strain, which can be written as:

$$\Gamma = \int_0^t \bar{\gamma}(t)dt \quad (3)$$

where  $\bar{\gamma}$  is the average shear rate during mixing. We can estimate this parameter from a calibration procedure established by Bousmina et al. [28]. In our case, the shear rate is correlated with the rotor speed  $N$  as follows:

$$\bar{\gamma} \approx 0.6 N \quad (4)$$

where the rotor speed is expressed in rpm.

### 3. Results and discussion

#### 3.1 Sisal fibers

First, we use sisal-based composites as an example to analyze in detail the evolution of fiber sizes, and then we apply this approach and results to composites with the other fibers. Figure 3 highlights, for a mixing time of 3 min, the changes of the weight average length and diameter of the fibers with the rotor speed. It is found that the fibers undergo a significant reduction in both length and diameter, already at low speed (50 rpm), indicating simultaneous phenomena of breakage and bundle dissociation. Above 50 rpm, the evolution is much slower and the morphology seems to stabilize. This effect of rotor speed at a fixed mixing time has already been observed by many authors [20-23, 29].

If now all the tests performed at different speeds and different mixing times are taken into consideration, a master curve can be obtained when the average length is plotted as a function of the specific mechanical energy,  $SME$  (Eq. (2), Figure 4a), or the cumulative strain,  $\Gamma$  (Eq. (3), Figure 4b). Despite some dispersion of the experimental data, due to the difficulty to accurately measure fibers' dimensions [24], the trend is clear. Fiber size evolution can be described by using exponential laws, as it was initially proposed for the breakage of glass fibers [30, 31] and more recently for lignocellulosic fibers [5, 27]:

$$L_w = L_\infty + (L_0 - L_\infty) \exp(-k_{L_{SME}} SME) \quad (5)$$

$$L_w = L_\infty + (L_0 - L_\infty) \exp(-k_{L_\Gamma} \Gamma) \quad (6)$$

where  $L_0$  is the initial fiber length,  $L_\infty$  is its ultimate length, and  $k_{L_{SME}}$  and  $k_{L_\Gamma}$  are the breakage constants, quantifying the breaking kinetics. As shown in Figures 4c,d and 4e,f, we can get similar results with the weight average diameter ( $D_w$ ) and the weight average aspect ratio  $((L/D)_w)$ , with the same types of fitting laws:

$$D_w = D_\infty + (D_0 - D_\infty) \exp(-k_{D_{SME}} SME) \quad (7)$$

$$D_w = D_\infty + (D_0 - D_\infty) \exp(-k_{D_r} \Gamma) \quad (8)$$

$$(L/D)_w = (L/D)_\infty + [(L/D)_0 - (L/D)_\infty] \exp[-k_{(L/D)SME} SME] \quad (9)$$

$$(L/D)_w = (L/D)_\infty + [(L/D)_0 - (L/D)_\infty] \exp[-k_{(L/D)\Gamma} \Gamma] \quad (10)$$

It is important to note that the evolution of the aspect ratio is not straightforward: for example, if the bundles separation is faster than the breakage, the aspect ratio may increase and its evolution will not be monotonous.

### 3.2 Strain or energy for the description of fiber size evolution?

From the previous results, we can infer that the choice of a pertinent descriptor to monitor fibers dimensional changes is not trivial. This is related to the fact that, for a given matrix, the specific energy is closely related to the cumulative strain, both depending on the average shear rate  $\bar{\dot{\gamma}}$  (Figure 5). In fact, the strain is proportional to  $\bar{\dot{\gamma}}$  while the energy varies as  $\bar{\dot{\gamma}}^{n+1}$ , where  $n$  is the index of the power law describing the evolution of the viscosity with the shear rate ( $\eta = K \bar{\dot{\gamma}}^{n-1}$ ).

To discriminate the two parameters, we prepared composites with a matrix having a lower viscosity and we measured fiber size distributions. As shown in Figure 5, this allows to obtain samples with the same strain, but different energies (for example, samples named A and B, with  $\Gamma = 45\ 000$  and  $SME = 422$  and  $278$  kWh/t, respectively), and samples with the same energy, but with different cumulative strain (for example, samples B and C, with  $SME$  about  $280$  kWh/t, and  $\Gamma = 45\ 000$  and  $30\ 600$ , respectively). These samples were analyzed in terms of fiber dimensions, and the results are given in Table 2. Samples A and B, at the same cumulative strain, have similar average size values, whereas samples B and C, at the same specific energy, are quite different. The sample C, characterized by the lowest strain value, is less degraded. It may be thus hypothesized that it is strain and not energy that governs fiber breakage.

Even though these first results seem pertinent, it would be more convincing to consider the whole size distributions and not only average values. To compare size distributions, it is customary to use the so-called "box-plot" or "box-and-whisker plot" representation [32]. As it can be seen in Figure 6, the box-plot can display in a single graph the different values of the distribution, such as the first decile (10% of total population), the lower quartile (25%), the median (50%), the upper quartile (75%), and the ninth decile (90%). On the same graph, we plot also the number average and the weight average values. Figure 7 presents the box-plots of length and diameter for samples A, B and C. They confirm that the size distributions of samples A and B (at the same cumulative strain) are very close, while those of samples B and C (at the same *SME*) are rather different. In particular, sample C that has undergone a lower level of cumulative strain shows a strong positive skew shape. Similar results (Figure S3 in Supplementary Data) were obtained for miscanthus. Therefore, if we want to use a single global parameter to describe lignocellulosic fiber size evolutions, we can conclude that the cumulative strain, rather than the specific energy, controls the size evolution of these fibers. This is, obviously, a simplification and the reality can be much more complex, as we saw through the rheo-optical observations in the Part 1 of these series [13]. It is not excluded that several, simultaneous or successive, mechanisms may exist, controlled by parameters which could be different (fiber composition, fiber morphology, etc.). However, our approach intends to propose a first-approximation description of the thermomechanical history undergone by the fibers, which can then be directly used to describe dimensional changes during compounding. For this reason, we will focus in the following on the cumulative strain.

### *3.3 Comparison of different types of fibers*

Figure 8a,b shows the size variations (length and diameter) for the retted hemp. Compared with sisal (Fig. 4d), a much faster dissociation of the bundles is observed: the diameter decreases from 346 to 60  $\mu\text{m}$  for a cumulative strain of 5000, corresponding approximately to 1 min of mixing at 150 rpm. This difference is due to the retting process, which weakens the "interfiber cement" and promotes the separation of the bundles [33-35]. Moreover, since the diameter of the bundles and their length do not change in the same way, it is not easy to predict what will be the evolution of the aspect ratio. In fact, as for the sisal shown in Figure 4f,  $L/D$  of retted hemp decreases also exponentially with the cumulative strain (Figure S4 in Supplementary Data). For the retted hemp, the strain must remain lower than 4 000 in order to keep interesting aspect ratio values (i.e. higher than 10).

Miscanthus, which showed a particular behavior under shear during rheo-optical observations [13], presents the same type of size evolution as the other fibers (Figure 8c,d and Figure S5 in Supplementary Data). This tends to confirm that, despite the variety of breakage mechanisms, the suggested description can be applied to most lignocellulosic fibers. However, the kinetics of miscanthus fiber size evolution is much slower than for retted hemp (compare  $L/D$  for hemp and miscanthus in Figs. S4 and S5, respectively). The reason is a different behavior under shear (peeling for miscanthus versus dissociation for hemp), as shown by rheo-optics [13].

So far, we have considered initially rather short fibers (2 to 3.5 mm). If initially longer fibers are used, such as, for example, flax fibers 12 mm long in average, we observed that they also demonstrate the same evolution of length, diameter, and aspect ratio (Figure S6 in Supplementary Data). However, if the evolution of the average diameter is similar to that of the short fibers species, the change in length is much faster:  $L$  is divided by more than 6 at a cumulative strain of 10 000, instead of a factor of 2 to 3

for the other fibers. The breakage is thus faster as the fibers are longer. This result is well known for rigid glass fibers [36].

All the results presented above confirm that we can propose the following evolution laws for fiber length, diameter and aspect ratio, based on cumulative strain, under the form of decreasing exponential functions:

$$L_w = L_\infty + (L_0 - L_\infty) \exp(-k_{L_r} \Gamma) \quad (6)$$

$$D_w = D_\infty + (D_0 - D_\infty) \exp(-k_{D_r} \Gamma) \quad (8)$$

$$(L/D)_w = (L/D)_\infty + [(L/D)_0 - (L/D)_\infty] \exp(-k_{(L/D)_r} \Gamma) \quad (10)$$

where  $k_{L_r}$ ,  $k_{D_r}$ ,  $k_{(L/D)_r}$  are breakage constants for length, diameter and aspect ratio, respectively. These constants obviously depend on the type of fiber considered.

In these expressions, the original dimensions ( $L_0$ ,  $D_0$ ,  $(L/D)_0$ ) are known *a priori*. The above results (Figures 5, 9 and S6) show that the final diameter ( $D_\infty \approx 60 \mu\text{m}$ ) and the final aspect ratio ( $(L/D)_\infty \approx 4.5$ , except for miscanthus which is lower) are weakly dependent on the botanical origin, in contrast to the final length, which ranges from 350  $\mu\text{m}$  for miscanthus to 650  $\mu\text{m}$  for flax. The final average diameter is always larger than that of a single elementary fiber, which varies from 10 to 20  $\mu\text{m}$  depending on the botanical origin. We can therefore conclude that bundles dissociation is never complete and that bundles of several elementary fibers are still present at the end of mixing.

The values of the different breakage constants ( $k_{L_r}$ ,  $k_{D_r}$ ,  $k_{(L/D)_r}$ ) calculated as the best fits of Eqs. (6), (8) and (10) to experimental data are indicated in Table 3. Several observations can be made:

- sisal is the fiber the length of which is the least sensitive to cumulative strain, whereas flax is the most sensitive. It seems that the length breakage constants are mainly determined by the initial length;

- dissociation of retted hemp is almost three times faster than that of other fibers;
- miscanthus is the fiber the aspect ratio of which is changing the least.

These results confirm the rheo-optical observations reported in Part 1 [13]. They show that not only the botanical origin of the fibers, but their initial dimensions and fiber treatment (retting) influence breakage constants which are the kinetic parameters describing size decrease during compounding.

To more easily compare the different types of fibers, we propose to define a "breakage index" for length, diameter and aspect ratio from the following expressions:

$$K_L = \frac{L_0 - L_w}{L_0} = \left(1 - \frac{L_\infty}{L_0}\right) \left[1 - \exp(-k_{L_r} \Gamma)\right] \quad (11)$$

$$K_D = \frac{D_0 - D_w}{D_0} = \left(1 - \frac{D_\infty}{D_0}\right) \left[1 - \exp(-k_{D_r} \Gamma)\right] \quad (12)$$

$$K_{L/D} = \frac{(L/D)_0 - (L/D)_w}{(L/D)_0} = \left(1 - \frac{(L/D)_\infty}{(L/D)_0}\right) \left[1 - \exp(-k_{(L/D)_r} \Gamma)\right] \quad (13)$$

These values range from 0 for the initial fiber to theoretically 1 for a fiber fully broken. Figure 9a compares the breakage indices of fibers in terms of length. Flax, hemp and miscanthus have similar kinetics, while for sisal it is significantly slower. The flax is the most sensitive (highest values of  $K_L$ ), followed by hemp, and then by miscanthus and sisal .

The diameter changes due to bundles dissociation are shown in Figure 9b. Dissociation of retted hemp bundles is very fast and significant (83%). Flax dissociation is also fast, but with a lower final value. The bundles of miscanthus and sisal are very difficult to separate, leading to lower values of  $K_D$  (0.66 for sisal).

Finally, the aspect ratio is presented in Figure 9c. For retted hemp and initially long flax fibers, the aspect ratio evolves a lot, reaching high values of  $K_{L/D}$ , around 0.89 for

flax and 0.74 for hemp. For sisal, and especially for miscanthus,  $L/D$  variations are more limited. These “breakage indices” are thus very useful to describe the evolution of the dimensions of lignocellulosic fibers and highlight the differences in fiber behavior depending on the botanical origin and initial size. These results are qualitatively consistent with the rheo-optical observations [13].

#### **4. Conclusions**

The dimensions of lignocellulosic fibers change through bundles dissociation and breakage, when subjected to a thermomechanical process, either during compounding or injection molding. In this paper, we quantified the changes in length, diameter and aspect ratio of different types of fibers, compounded with an internal mixer, by systematically varying the processing conditions. We showed that dimensions’ evolutions can be described using decreasing exponential functions of the cumulative strain received by the fibers. These size changes partly depend on the botanical origin, but also on the initial dimensions of the fibers: the longer they are, the more they will break. The kinetics of the size evolution may be described by a “breakage index” that efficiently discriminates the behavior of the various fibers. We can conclude that, for all types of fibers studied, it is advisable to keep strain levels largely below 5 000 (in the sense that we have defined on the internal mixer) in order to preserve high fiber lengths which is required for composite mechanical reinforcement.

#### **Acknowledgements**

The results presented in this paper were obtained during the DEFIBREX project, funded by the French National Research Agency (ANR-12-RMNP-004). We thank our colleagues S. Dobosz (INRA), J. Beaugrand (INRA), F. Berzin (INRA) for their

collaboration, as well as the company FRD<sup>®</sup> (Fibre Recherche Développement<sup>®</sup>, Troyes, France) for providing the fibers.

## References

- [1] Ausias G, Bourmaud A, Coroller G, Baley C. Study of the fibre morphology stability in polypropylene-flax composites. *Polym Deg Stab* 2013;98:1216-1224.
- [2] Doumbia AS, Castro M, Jouannet D, Kervoëlen A, Falher T, Cauret L, Bourmaud A. Flax/polypropylene composites for lightened structures: Multiscale analysis of process and fibre parameters. *Mat Design* 2015;87:331-341.
- [3] Müssig J. *Industrial Applications of Natural Fibres*. Chichester: John Wiley, 2010.
- [4] Thumm A, Dickson AR. The influence of fibre length and damage on the mechanical performance of polypropylene/wood pulp composites. *Compos Part A* 2013;46:45–52.
- [5] Beaugrand J, Berzin F. Lignocellulosic fiber reinforced composites: influence of compounding conditions on defibrization and mechanical properties. *J Appl Polym Sci* 2013;128:1227-1238.
- [6] Hornsby PR, Hinrichsen E, Tarverdi K. Preparation and properties of polypropylene composites reinforced with wheat and flax straw fibres. Part II Analysis of composite microstructure and mechanical properties. *J Mat Sci* 1997;32:1009-1015.
- [7] Bos HL, Müssig J, van den Oever MJA. Mechanical properties of short-flax-fibre reinforced compounds. *Comp Part A* 2006;37:1591-1604.
- [8] Barkoula NM, Garkhail SK, Peijs T. Effect of compounding and injection molding on the mechanical properties of flax fiber polypropylene composites. *J Reinf Plast Comp* 2010;29:1366-1385.
- [9] Feng Y, Zhang D, Qu J, He H, Xu B. Rheological properties of sisal fiber/poly(butylene succinate) composites. *Polym Test* 2011;30:124-130.

- [10] Peltola H, Pääkkönen E, Jetsu P, Heinemann S. Wood based PLA and PP composites: Effect of fibre type and matrix polymer on fibre morphology, dispersion and composite properties. *Comp Part A* 2014;61:13-22.
- [11] Dickson AR, Even D, Warnes JM, Fernyhough A. The effect of reprocessing on the mechanical properties of polypropylene reinforced with wood pulp, flax or glass fibre. *Comp Part A* 2014;61:258-267.
- [12] Feldmann M, Heim HP, Zarges JC. Influence of the process parameters on the mechanical properties of engineering biocomposites using a twin-screw extruder. *Comp Part A* 2016;83:113-119.
- [13] Castellani R, Di Giuseppe E, Dobosz S, Beaugrand J, Berzin F, Vergnes B, Budtova T. Lignocellulosic fiber breakage in a molten polymer. Part 1. Qualitative analysis using rheo-optical observations. Under revision in *Comp Part A* (2016).
- [14] Baley C. Influence of kink bands on the tensile strength of flax fibers. *J Mater Sci* 2004;39:331–334.
- [15] Le Duc A, Vergnes B, Budtova T. Polypropylene/natural fibres composites: analysis of fibre dimensions after compounding and observations of fibre rupture by rheo-optics. *Comp Part A* 2011;42:1727-17370.
- [16] Hughes M. Defects in natural fibres: their origin, characteristics and implications for natural fibre-reinforced composites. *J Mater Sci* 2011;47:599–609.
- [17] Terenzi A, Kenny JM, Barbosa SE. Natural fiber suspensions in thermoplastic polymers. I. Analysis of fiber damage during processing. *J Appl Polym Sci* 2007;103:2501-2506.
- [18] Santos PA, Spinace MAS, Feroselli KKG, De Paoli MA. Polyamide-6/vegetal fiber composite prepared by extrusion and injection molding. *Comp Part A* 2007;38:2404-2411.

- [19] Le Moigne N, van den Oever M, Budtova T. A statistical analysis of fibre size and shape distribution after compounding in composites reinforced by natural fibres. *Comp Part A* 2011;42:1542-1550.
- [20] Quijano-Solis C, Yan N, Zhang SY. Effect of mixing conditions and initial fiber morphology on fiber dimensions after processing. *Comp Part A* 2009;40:351-358.
- [21] Joseph PV, Joseph K, Thomas S. Effect of processing variables on the mechanical properties of sisal-fiber-reinforced polypropylene composites. *Comp Sci Tech* 1999;59:1625-1640.
- [22] Baiardo M, Zini E, Scandola M. Flax fibre-polyester composites. *Comp Part A* 2004;35:703-710.
- [23] Iannace S, Ali R, Nicolai L. Effect of processing conditions on dimensions of sisal fibers in thermoplastic biodegradable composites. *J Appl Polym Sci* 2001;79:1084-1091.
- [24] Di Giuseppe E, Castellani R, Dobosz S, Malvestio J, Berzin F, Beaugrand J, Delisée C, Vergnes B, Budtova T. Reliability evaluation of automated analysis, 2D scanner, and micro-tomography methods for measuring fiber dimensions in polymer-lignocellulosic fiber composites. *Comp Part A* 2016;90:320-329.
- [25] El-Sabbagh AMM, Steuernagel L, Meiners D, Ziegmann G. Effect of extruder elements on fiber dimensions and mechanical properties of bast natural fiber polypropylene composites. *J Appl Polym Sci* 2014;40435.
- [26] Sojoudiasli H, Heuzey MC, Carreau PJ. Rheological, morphological and mechanical properties of flax fiber polypropylene composites: influence of compatibilizers. *Cellulose* 2014;21:3797–3812.

- [27] Berzin F, Vergnes B, Beaugrand J. Evolution of lignocellulosic fibre lengths along the screw profile during twin screw compounding with polycaprolactone. *Comp Part A* 2014;59:30-36.
- [28] Bousmina M, Ait-Kadi A, Faisant JB. Determination of shear rate and viscosity from batch mixer data. *J Rheol* 1999;43:415-433.
- [29] Teuber L, Militz H, Krause A. Processing of wood plastic composites: The influence of feeding method and polymer melt flow rate on particle degradation. *J Appl Polym Sci* 2015;43231:1-9.
- [30] Shon K, Liu D, White JL. Experimental studies and modeling of development of dispersion and fiber damage in continuous compounding. *Intern Polym Proc* 2005;20:322–331.
- [31] Inceoglu F, Ville J, Ghamri N, Durin A, Valette R, Vergnes B. Correlation between processing conditions and fiber breakage during compounding of glass fiber-reinforced polyamide, *Polym Comp* 2011;32:1842-1850.
- [32] Tukey JW. Box-and-Whisker Plots. In: Reading MA, editor. *Exploratory Data Analysis*. Addison-Wesley, 1977. p.39-43.
- [33] Sharma HSS, Van Sumere CF. *The Biology and Processing of Flax*. Belfast: M. Publications, 1992.
- [34] Akin DE, Foulk JA, Dodd RB, McAlister III DD. Enzyme-retting of flax and characterization of processed fibers. *J Biotechnol* 2001;89:193–203.
- [35] Meijer WJM, Vertregt N, Rutgers B, Van de Waart M. The pectin content as a measure of the retting and rettability of flax. *Ind Crops Prod* 1995;4:273–284.
- [36] Durin A, De Micheli P, Ville J, Inceoglu F, Valette R, Vergnes B. A matricial approach of fibre breakage in twin-screw extrusion of glass fibres reinforced thermoplastics. *Compos Part A* 2013;48:47–56.

## Figure captions

- Figure 1. Incorporation and mixing of hemp fibers in the matrix HP400R. Time evolution of (a) torque and temperature, and (b) mechanical energy.
- Figure 2. Evolution of the final temperature with mixing time and rotor speed (sisal, PPH5060).
- Figure 3. Changes in (a) weight average length and (b) weight average diameter with the rotor speed for a mixing time of 3 min (sisal, PPH5060); the lines are given to guide the eye.
- Figure 4. Changes in weight average length (a, b), diameter (c, d) and aspect ratio (e, f) with the specific energy (left) and the cumulative strain (right) (sisal, PPH5060); lines represent fits by Eqs. (5) - (10).
- Figure 5. Relationship between the specific energy and the cumulative strain for composites made with the two matrices (sisal).
- Figure 6. (a) Example of frequency size distribution (left) and related "box-and-whisker" representation (right).
- Figure 7. "Box-and-whisker" plots for (a) the length and (b) the diameter of sisal based composites, samples A, B and C. Triangles correspond to number average and circles to weight average values. For some samples, the weight average values are out of the domain of the figure (see Table 2).
- Figure 8. Changes in weight average length (left) and weight average diameter (right) with the cumulative strain for retted hemp, PPH5060 (a, b) and miscanthus, PPH5060 (c, d); lines represent fits by Eqs. (6) and (8).
- Figure 9. Evolution of the "breakage index" of the weight average (a) length, (b) diameter, and (c) aspect ratio with the cumulative strain for different fibers.

Table 1. Weight average values of length ( $L_w$ ), diameter ( $D_w$ ) and aspect ratio ( $(L/D)_w$ ) of the initial fibers, and their composition (hemicellulose and lignin contents, data taken from reference [13]).

Fiber	$L_w$ (mm)	$D_w$ ( $\mu\text{m}$ )	$(L/D)_w$ (-)	Hemicellulose (%)	Klason lignin (%)
Retted hemp	3.49	346	16.8	10.5	5.7
Miscanthus	1.91	240	4.3	26.8	21.6
Sisal	3.5	177	11	25.2	9.3
Flax	12.0	250	41.9	8.6	4.9

Table 2. Processing conditions ( $SME$  and cumulative strain  $\Gamma$ ) and weight average values of length ( $L_w$ ), diameter ( $D_w$ ) and aspect ratio ( $(L/D)_w$ ) of the samples A, B and C (see Figure 5).

Sample	$SME$ (kWh/t)	$\Gamma$ (-)	$L_w$ (mm)	$D_w$ ( $\mu\text{m}$ )	$(L/D)_w$ (-)
A	422	45 000	0.598	56	5.4
B	278	45 000	0.643	64	4.3
C	285	30 600	1.047	91	4.9

Table 3. Values of breakage constants for the length ( $k_{L_r}$ ), diameter ( $k_{D_r}$ ) and aspect ratio ( $k_{(L/D)_r}$ ) of the fibers studied.

Fiber	$k_{L_r}$	$k_{D_r}$	$k_{(L/D)_r}$
Retted hemp	$1.8 \cdot 10^{-4}$	$5.0 \cdot 10^{-4}$	$2.0 \cdot 10^{-4}$
Miscanthus	$1.5 \cdot 10^{-4}$	$1.5 \cdot 10^{-4}$	$0.5 \cdot 10^{-4}$
Sisal	$1.0 \cdot 10^{-4}$	$1.5 \cdot 10^{-4}$	$1.8 \cdot 10^{-4}$
Flax	$2.2 \cdot 10^{-4}$	$3.5 \cdot 10^{-4}$	$2.2 \cdot 10^{-4}$

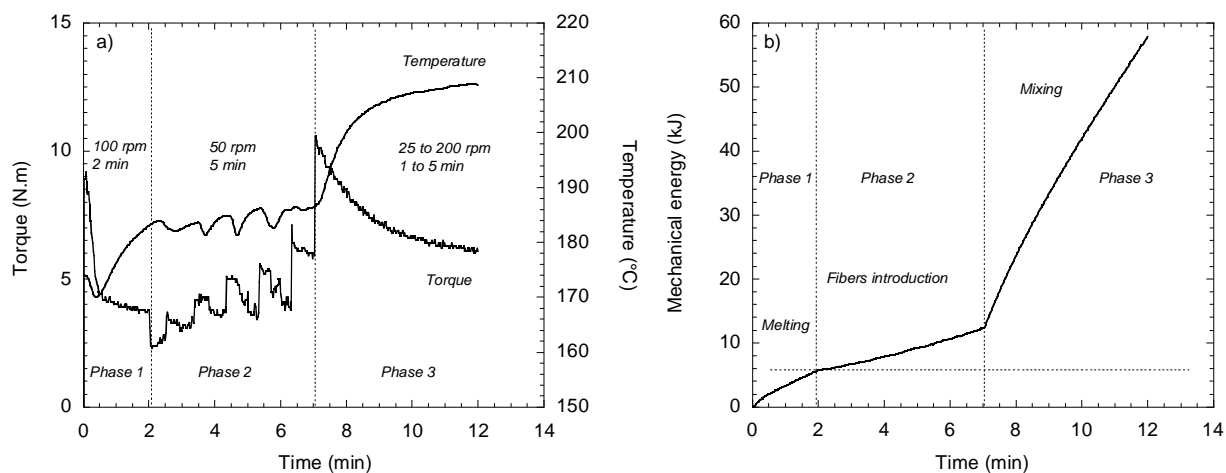


Figure 1. Incorporation and mixing of hemp fibers in the matrix HP400R. Time evolution of (a) torque and temperature, and (b) mechanical energy.

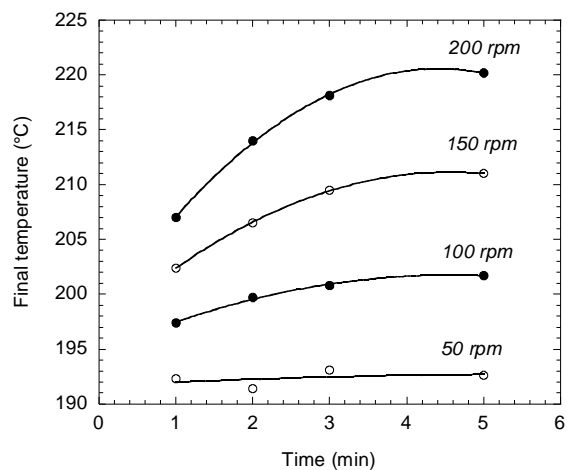


Figure 2. Evolution of the final temperature with mixing time and rotor speed (sisal, PPH5060)

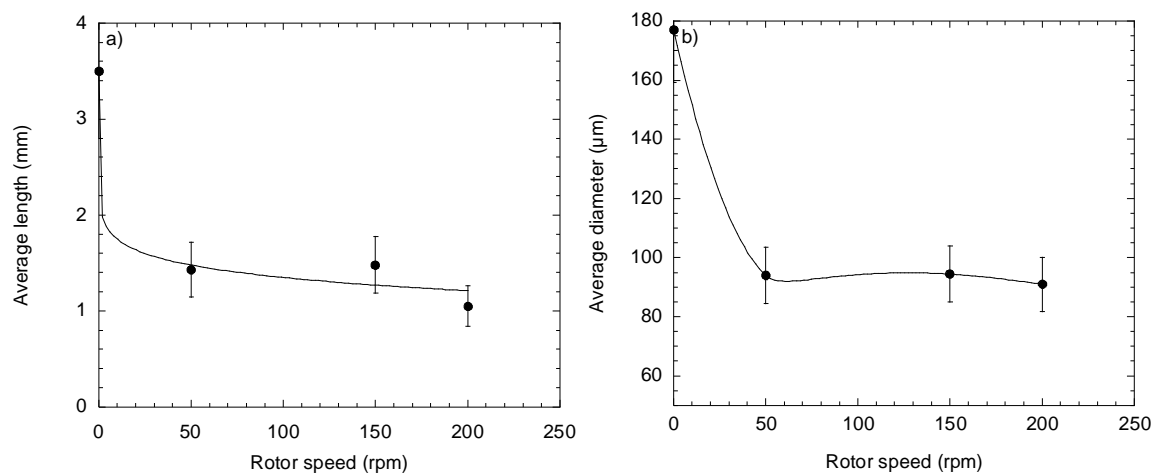


Figure 3. Changes in (a) weight average length and (b) weight average diameter with the rotor speed for a mixing time of 3 min (sisal, PPH5060); the lines are given to guide the eye.

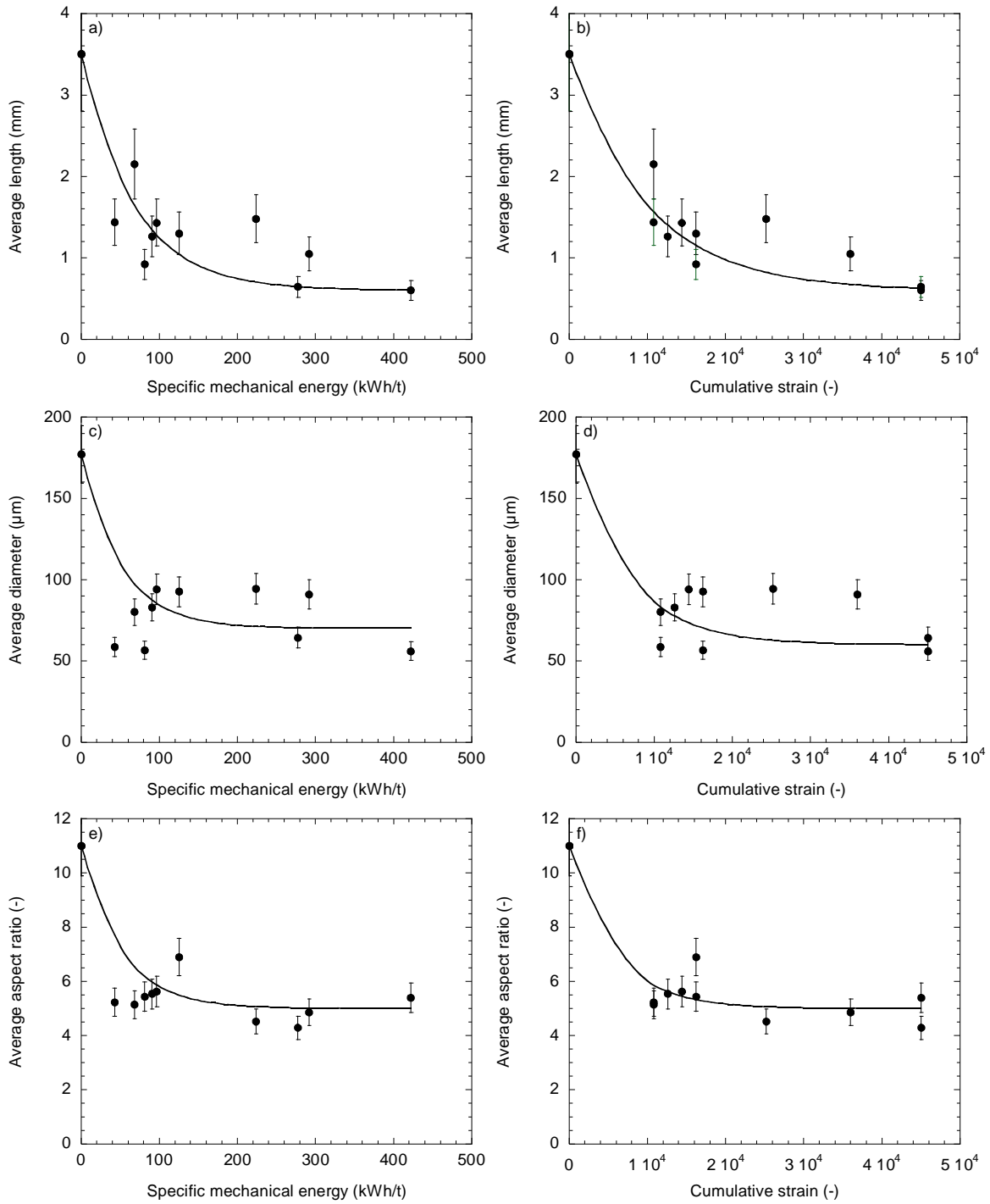


Figure 4. Changes in weight average length (a, b), diameter (c, d) and aspect ratio (e, f) with the specific energy (left) and the cumulative strain (right) (sisal, PPH5060); lines represent fits by Eqs. (5) - (10).

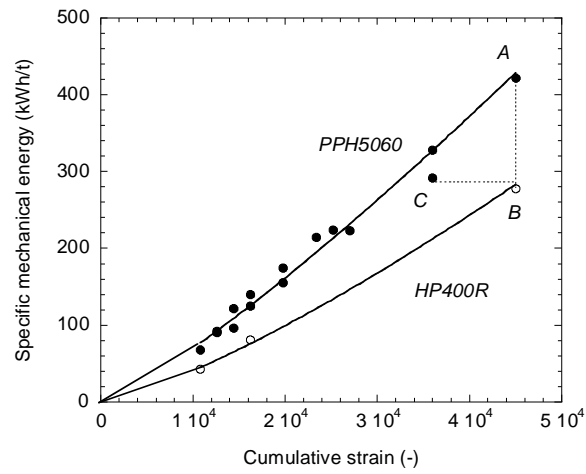


Figure 5. Relationship between the specific energy and the cumulative strain for composites made with the two matrices (sisal).

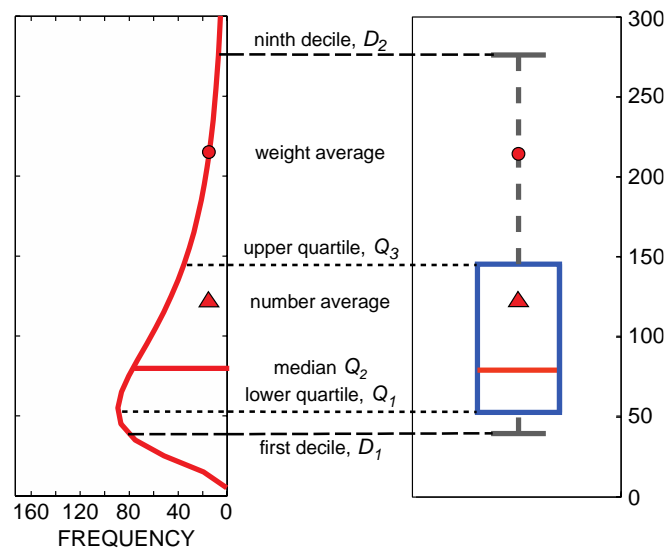


Figure 6. Example of frequency size distribution (left) and related “box-and-whisker” representation (right).

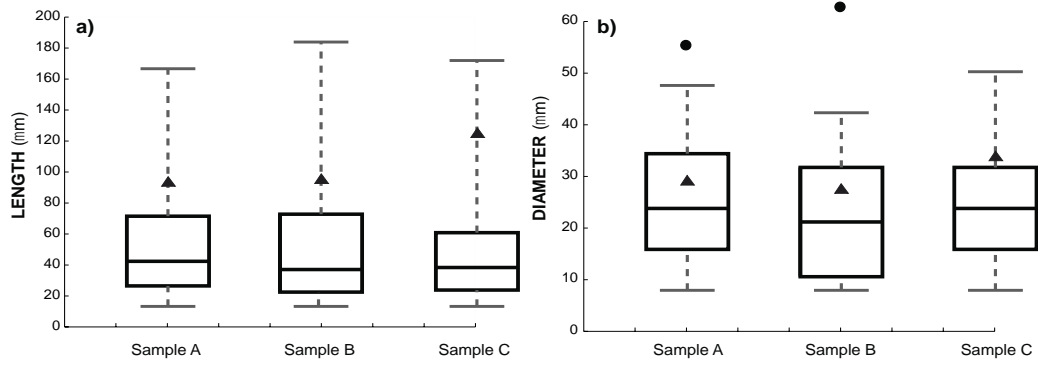


Figure 7. "Box-and-whisker" plots for (a) the length and (b) the diameter of sisal based composites, samples A, B and C. Triangles correspond to number average and circles to weight average values. For some samples, the weight average values are out of the domain of the figure (see Table 2).

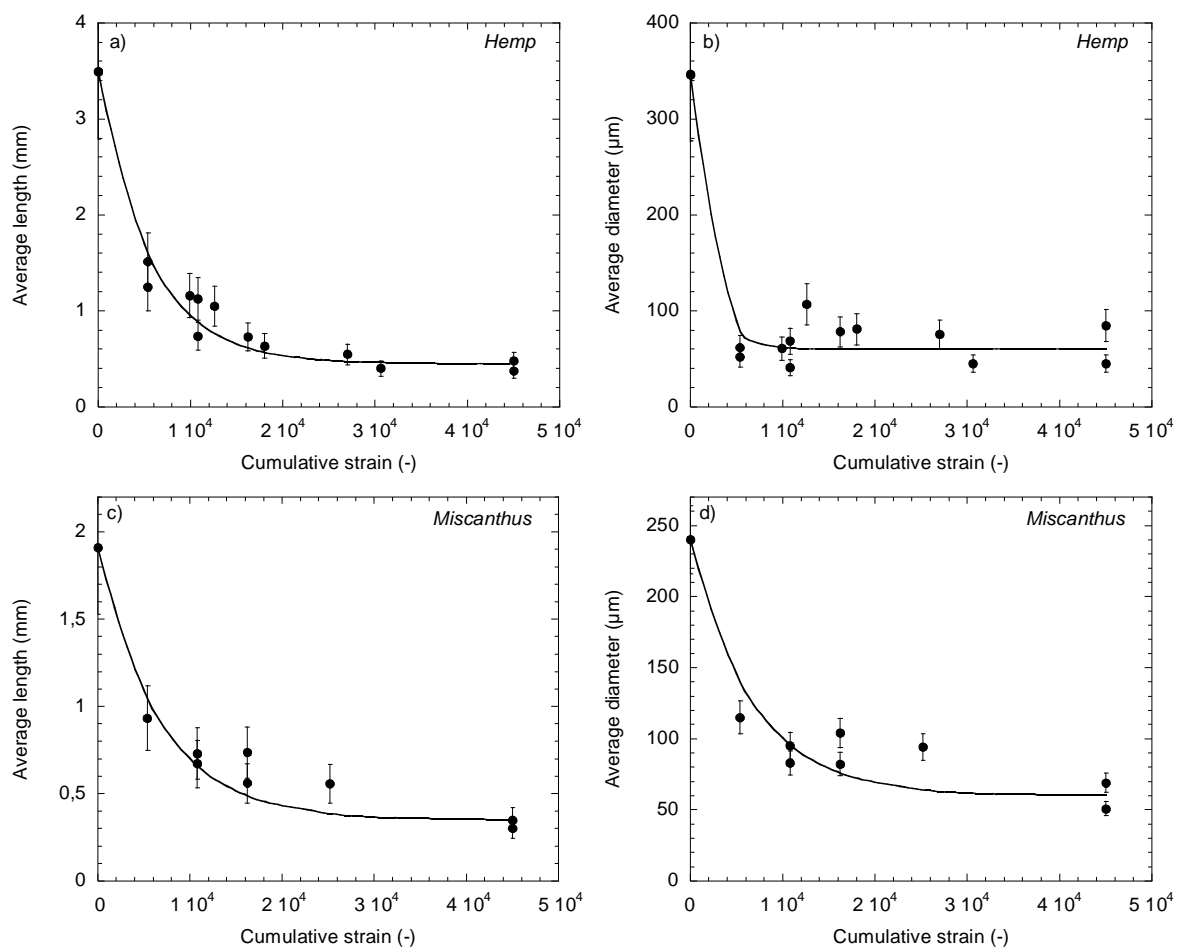


Figure 8. Changes in weight average length (left) and weight average diameter (right) with the cumulative strain for retted hemp, PPH5060 (a, b) and miscanthus, PPH5060 (c, d); lines represent fits by Eqs. (6) and (8).

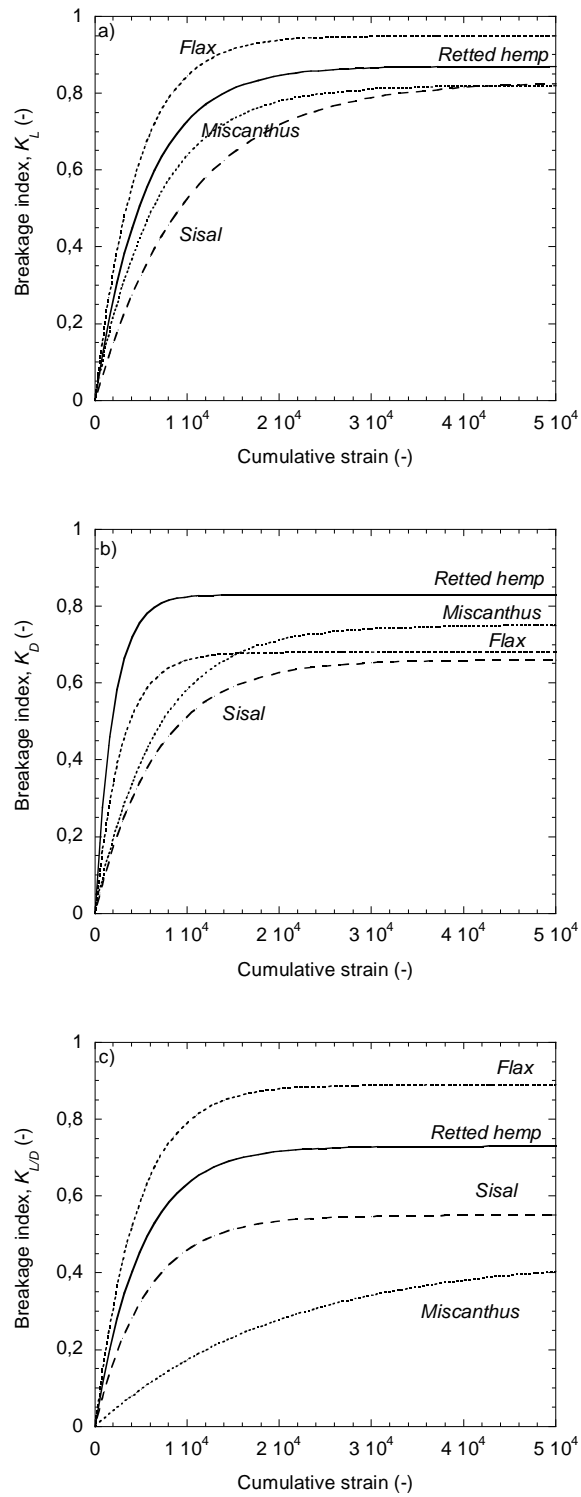


Figure 9. Evolution of the “breakage index” of the weight average (a) length, (b) diameter, and (c) aspect ratio with the cumulative strain for different fibers.